Trapping of biomolecular ions generated by Infra-red laser desorption on microdroplets under vacuum

Nicolas Nieuwjaer, Ali Beydoun, Rolando Lozada Garcia, Serge-Daniel Leite, Frédéric Lecomte, Charles Desfrançois, Albert Kaladjian, Gilles Grégoire

Trapping of biomolecular ions generated by Infra-red laser desorption on microdroplets under vacuum.

Nicolas Nieuwjaer, Ali Beydoun, Rolando Lozada Garcia, Serge-Daniel Leite, Frédéric Lecomte, Charles Desfrançois, Albert Kaladjian, Gilles Grégoire*, Bruno Manil.

Université Sorbonne Paris Nord, Lab. de Physique des Lasers, CNRS, 93430 Villetaneuse, France

*present adress : Université Paris-Saclay, CNRS, Institut des Sciences Moléculaires d'Orsay, F-91405 Orsay, France

Abstract. A droplet beam-laser ablation mass spectrometer has been developed for the isolation of ions ejected from a liquid droplet under vacuum. After desorption from the droplet, the ions are mass-analysed with a home-made Time-of-Flight spectrometer, either by a delayed extraction line or by coupling of the desorption source with a Paul trap. The ability of this set-up to equaly work in the positive and negative modes, and to preserve small non-covalent complexes in the gas phase, is analysed. The effects of the broad initial velocity distribution and of the collisional path of the ejected ions in the dense desorption area are discussed. We prove the feasibility of the coupling of the desorption source with a Paul trap and our first results clearly indicate the ability of this coupling to escape from the initial velocity distribution.

1 – Introduction

The transfer of large biomolecules into the gas phase has been impractical for a long time. In the 1980s, intact biomolecular ions were produced by new "soft" desorption/ionization methods : Fast Atom Bombardment[1,2] (FAB), ElectroSpray Ionization[3,4] (ESI) and Matrix-Assisted Laser Desorption[5,6] (MALDI). Nowadays, native-ESI Mass Spectrometry (MS) is heavily used in studies of non-covalent interactions and to understand the architecture of biomolecular complexes[7-12]. MALDI-MS is a viable alternative to native ESI-MS to study biomolecular complexes : fine-tuned conditions, including proper choice of matrix, solvent, pH, concentrations and laser energy, allow to preserve the non-covalent interactions[13-16]. However, the analysis of biomolecular complexes using ESI or MALDI-MS is not yet routine[17], each biomolecular complex requiring its own specific protocol. In the transition from solution to gas phase during ESI, biomolecules experience vastly different physicochemical environments that can potentially affect their structure[18]. ESI-MS is also sensitive to salts and

is largely incompatible with detergents and, during isolation procedures, weak interactions are easily lost. MALDI-MS can yield stoichiometric information in high salt environments, above all if interacting species can be artificially stabilized by chemical crosslinking[19,20], but it generates ions from the solid phase (and with poorely biologically pertinent matrices) and they often no longer exist under "native" conditions. Different experimental methods have then been developed to overcome these disagreements, with the underlying idea to desorb biomolecules directly from liquid water under vacuum.

In the 1990s, small peptides[21] and proteins[22] were generated from frozen ice matrixes by infrared MALDI, but it was found that bulk frozen water ice was a poor matrix that produced mass spectra with low signal-to-noise ratio and poor mass resolution[23]. In the meantime, the liquid beam technique under vacuum was developed[24-29], and it was combined with multi-photon ionization and time-of-flight mass spectrometry by Kondow and co-workers to eject and analyse cluster ions directly from a liquid beam[30-32]. In 1996, a novel liquid-phase bioanalytical method, named Laser-Induced Liquid Beam Ionization/Desorption, has been proposed by Brutschy and co-workers[33,34] : an infrared laser tuned to the OH stretch vibration of liquid water enables a very soft desorption of protonated or ionic aggregates of supra-molecular species from liquid beams directly under vacuum. This technique, also named Free Liquid Matrix Assisted Laser Dispersion of Ions or Ionic aggregates by the Abel's group[35], has the ability to generate low-charge molecular ions and associated complexes of biomolecules from "bulk water" under vacuum[36-44]. Nevertheless, the use of liquid beams implies high sample consumption, which is an important drawback for biomolecular studies, and also requires high pumping capacities, which generates impractical experimental set-ups. To overcome these two difficulties, the liquid beam has been pulsed in order to be changed into a train of liquid droplets. This method was explored in 2006 by Brutschy and co-workers[45] and by Kohno and co-workers[46] : droplets with a few tens of micrometers diameter are irradiated directly under vacuum to generate biomolecular ions which are subsequently analysed by Time of Flight (ToF) mass spectrometry. Similarly to Aerosol IR-MALDI[47], continuous flow IR-MALDI[48,49], or Atmospheric Pressure IR MALDI[50-52], the IR ablation of these droplets is a soft desorption method which might be interfaced with liquid chromatography and has several favorable characteristics, including ionization without any additional matrices and tolerance to contaminants such as detergents and buffer salts. Laser Induced Liquid Bead Ion Desorption (LILBID) has been applied successfully to the analysis of membrane proteins[53-56] and

oligonucleotides[57,58] and very recent studies underline the interest of this technique for structural biology[59-65]. Nevertheless, the mechanism for IR ablation of the droplets is not fully understood. It is presumed to be either a thermal process by local heating of the liquid or a mechanical one due to a shock wave[66,67], depending on the energy and on the penetration depth of the laser excitation. Various models have been proposed to describe the isolation mechanism of solute molecules into the gas phase subsequently to the IR radiation absorption. Brutschy and co-workers proposed a "lucky survivor" model[33,53] in which ions are liberated from the solution in a gaseous plume with a supercritical phase and then suffer from recombination from counterions simultaneously produced in the plume. Another model was proposed by Abel and co-workers. In this nanodroplet model[35,44], inhomogeneous heating, spinodal decomposition and shock wave formation produces a highly efficient dispersion of the liquid and the formation of nano-droplets with embedded biomolecules and ions. The evaporation of charged nanodroplets then leads to the product ions in the gas phase. This latter model is supported by molecular dynamic simulations for atomic and molecular clusters impulsively excited[68,69], by velocity measurements of water clusters produced from a liquid beam[70] and by a study of the gas-phase charge distribution obtained by IR laser ablation of a droplet beam[71].

The experimental set-up that we present here aims to gain insight into these mechanisms of isolation of ions in the gas phase susbequently to IR irradiation of microdroplets under vacuum, and to improve the mass resolution of LILBID. After the IR irradiation of the droplets, ions are extracted either by a delayed line extraction or by an innovative coupling with a Paul trap. Such a coupling was proposed by Kohno and co-workers[72], with an irradiation of the droplets inside the trap but, in our set-up, we trap the product ions after an external irradiation of the droplets. This results in an improved mass resolution and the observation of hydrated product ions in addition to the isolated species. We have studied different molecules of biological interest with this device and we discuss the influence of the different experimental parameters.

2 – Experimental

The experimental device is constituted of three main parts : a desorption source to transfer biomolecules into the gas phase, an extraction area to collect ions produced by the desorption source, and a ToF mass spectrometer to mass analyse these ions. In a first section, we will describe the desorption source whose principle lies on the irradiation of microdroplets directly under vacuum. In a second part, we will describe the coupling of this source with pulsed ion extraction. In a third part, an alternative experimental set-up in which the pulsed ion extraction is replaced by a Paul Trap will be described.

2.1 - Desoprtion source.

As in LILBID, our desorption source is based on the desorption of liquid microdroplets by an IR laser directly under vacuum. The microdroplets (diameter = 50 μm) are produced on demand, at a frequency of 20 Hz, by a droplet generator (MD-K-130 from Microdrop Technologies GmbH, Norderstedt, Germany). This generator does not work under vacuum where it ultimately freezes due to strong evaporative cooling. It is then housed in a pumped chamber (generator chamber, marked as chamber "1" on figure 1), and the droplets are introduced by differential pumping stages into a lower pressure chamber (main desorption chamber, marked as chamber "3" on figure 1), through two skimmers : the first one (diameter = 300 μm) separates the generator chamber from an intermediate chamber (chamber "2" on figure 1) and the second one (diameter = 500 μm) separates the intermediate chamber from the main desorption chamber in which the droplet will be irradiated by an IR laser. This last chamber is pumped at a pressure of hardly less than 10^{-5} mbar by a main turbomolecular tump. The intermediate chamber is pumped at a pressure of a little less than 10^{-1} mbar through the second skimmer but also directly by a small turbomolecular pump. The generator chamber is pumped through the first skimmer, and a microleak valve allows to adjust the pression in this chamber (routinely, the pression in the generator chamber is around 280 mbar). The droplet generator is mounted on a piezo-driven device which allows to align it with the axis of the two skimmers and to compensate for different droplet ejection modes. Several CCD cameras and pulsed diodes allow to stroboscopically visualize the droplet just after its ejection and above each of the two skimmers, in order to finely tune the position and the orientation of the

droplet generator. The droplet can also be visualized in the area of interaction with the IR laser, which allows to ascertain the droplet irradiation. Once the droplets are in the main desoprtion chamber, they are irradiated by nanosecond mid-IR laser pulses generated by a home-made optical parametric oscillator. Namely, a lithium niobate crystal is pumped by a nanosecond pulsed Nd:YAG laser at a wavelength of 1,064 μm (13 MW/cm^2) and the idler wavelength can be tuned between 2.4 and 4 μm (with a large spectral width, around 50 cm^{-1}), with an energy up to 5 mJ per pulse. The laser beam is focused with a lens located inside the main desorption chamber, 10 cm upstream of the interaction area with the droplet, and the cross-section is approximately of 0.04 mm^2, which corresponds to an irradiance of 25 MW/cm^2 for an energy of 1 mJ. The laser is pulsed at 20 Hz, which then sets the frequency of the droplets generator to the same frequency so that each microdroplet is irradiated.

The studied biomolecules (bradikinin, vancomycin, N$^{\alpha}$,N$^{\varepsilon}$-diacetyl-L-Lys-D-Ala-D-Ala, Tryptophan Zipper TZ4) were purchased from Merck and used with no further purification. They were disolved at micromolar concentrations in a mixture of water and dimethylsulfoxide (DMSO) whose proportions will be discussed in section 3. The tank, connected to the droplet generator, is housed in the first chamber at a pressure of 280 mbar.

2.2 Coupling of the desorption source with pulsed ion extraction.

Ions generated during the irradiation of the droplet are extracted and mass analysed by coupling the desorption source with pulsed ion extraction and a ToF mass spectrometer. The overall experimental set-up is schematically represented in figure 1. The desorption laser is focused on the droplets on their trajectory between the two first electrodes of a delayed extraction line, as described by Wiley and McLaren[73] and commonly used in MALDI[74-76]. This line is here constituted of four electrodes. The first one (on the left of the droplet trajectory on figure 1) is holded at a continuous potential. The two following ones (on the right of the droplet trajectory on figure 1) are pulsed electrodes and the last one is grounded. The continuous accelerating field applied between the first and fourth electrodes is typically of a few hundred of volts per centimeter, and the pulsed accelerating field applied during 1 μs between the second and third electrodes is typically of 2-3 thousand of volts per centimeter and is delayed by few microseconds as compared with the laser pulse, allowing the

acceleration and subsequent mass analysis of a fraction of the total velocity distribution of the desorbed species. Typical values of the different applied potentials are given in table I.

Electrode	1 (continuous plate)	2 (first pulsed grid)	3 (second pulsed grid)	4 (grounded grid)	Einzel lens
Potential (V)	-222	0/-2900	0/-2200	0	-832
Position (mm)	-7	7	19	31	68

Table I : Positions and voltage values of the different electrodes composing the delayed extraction line. The electrodes are labelled as described in the experimental section. The electrodes are located with respect to the position at which the IR laser ablation of the droplet takes place. The position of the Einzel lens corresponds to the position of the central part of this lens, which is 35 mm long. The voltages are the ones used in Figure 10 for the comparison with the SIMION simulations. The pulse applied to the second and third electrode is 1 µs long and is time delayed of 9 µs as compared with the laser pulse.

The fourth electrode marks the beginning of the free flight path which is about 70 cm long. Two einzel lenses allow to focus the beam throught a skimmer separating the main desoprtion chamber and the detection chamber (at a pressure of 10^{-6} mbar), and then on a microchannel plates detector. A set of deflectors is used to compensate for mechanical misalignement between the two chambers. Ions are post-accelerated by a 500 V voltage just before the front face of the microchannel plates. Mass spectra are acquired after amplification with a digital oscilloscope and transferred to a microcomputer for analysis. The whole set-up can be adapted for positive or negative ions detection.

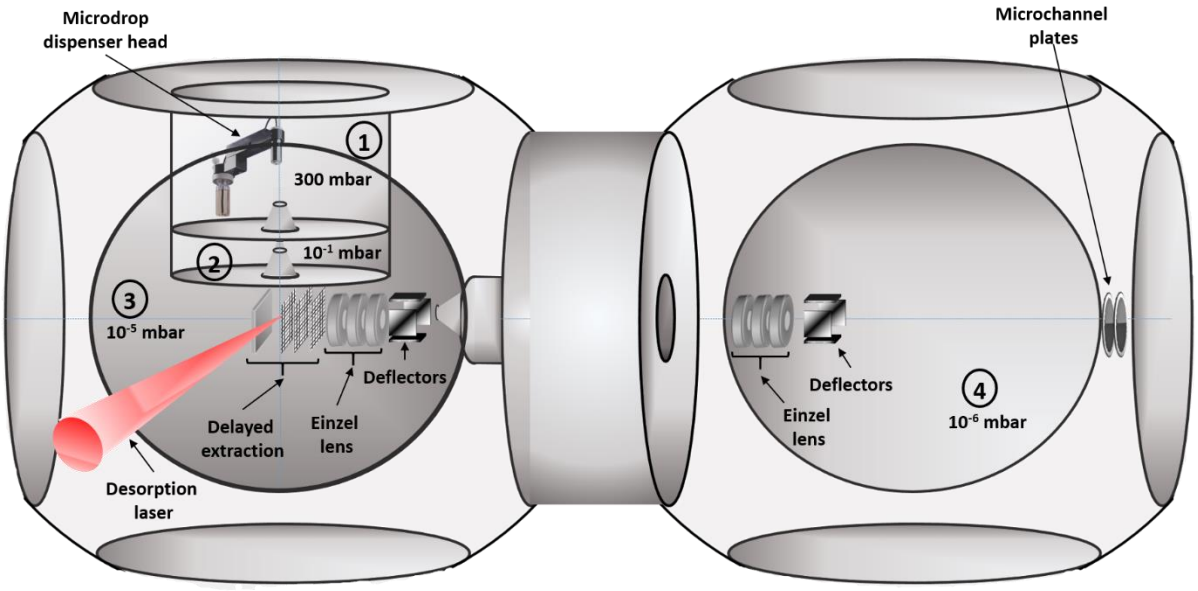

Figure 1 : Schematic view of the coupling of the desorption source with pulsed ion extraction. The four chambers are labelled 1 to 4 (1: generator chamber, 2: intermediate chamber, 3:main desoprtion chamber, 4:detection chamber).

2.3 Coupling of the desorption source with a Paul trap.

As it will be discussed later, the delay line extraction described above is a first improvement for a better mass resolution but it does not allow to sufficiently compensate for the broad velocity distribution consequent to the IR ablation of the droplets. We have then modified our extraction set-up in order to make it more independent from these broad initial conditions. This was done by coupling the IR irradiation of the droplet with a Paul trap (Jordan TOF Products, Inc.). A first electrode, located a few millimeters upstream the crossing point of the droplet trajectory with the IR laser beam, is maintained at a constant potential (typically 2 kV). The entrance end cap electrode of the trap is located a few millimeters downstream this same crossing point, as shown in Figure 2. The whole trap is biased at a potential which is a few volts smaller (typically three or four volts smaller) than the one of the first electrode. This potential difference is adjusted in order to reduce the speed of ions coming into the trap. Helium is injected into the trap via a pulsed valve a few hundred of microseconds before the droplet ablation. A radio frequency (RF) voltage (typically 900 V for m/z 1000) is applied to the ring electrode which traps the product ions. After a certain duration (between 0 and 50 ms, which is the period of the microdroplet dispenser and of the IR laser), the trapped ions are accelerated by a pulsed electric field applied to the endcap electrodes : a potential difference of $\pm$400 V is applied 4 μs after the RF field was turned off to avoid deflection of ions. Ions are then accelerated between the exit endcap electrode of the trap and the first electrode of an einzel lens (located at 2 cm from the end cap). The ion detection is realized with a microchannel plates detector, with a 10 kV post-acceleration, after a free flight path which is about 90 cm long. The pressure in the detection chamber is less than 10^{-6} mbar. The pressure in the desorption chamber is between 5 10^{-6} and 9 10^{-6} depending on the opening of the pulsed valve injecting helium into the trap as shown in table II, which corresponds to the upper limit for the trap functionment.

Pressure (mbar)	Generator chamber	Intermediate chamber	Desorption chamber	Detection chamber
Droplet generation	280	$8\ 10^{-2}$	$2\ 10^{-6}$	$8\ 10^{-7}$
Droplet generation + desorption	280	$8\ 10^{-2}$	$5\ 10^{-6}$	$8\ 10^{-7}$
Droplet generation, desorption + trapping	280	$8\ 10^{-2}$	$9\ 10^{-6}$	$8\ 10^{-7}$

Table II : measured pressures in the four chambers of the set-up for different functioning modes. The first line corresponds to the microdroplet generator alone, the second line corresponds to the adding of the laser desorption, and the third line corresponds to the adding of the trapping of the product ions with the 190 µs long opening of the pulsed valve at each cycle (with a 50 ms period).

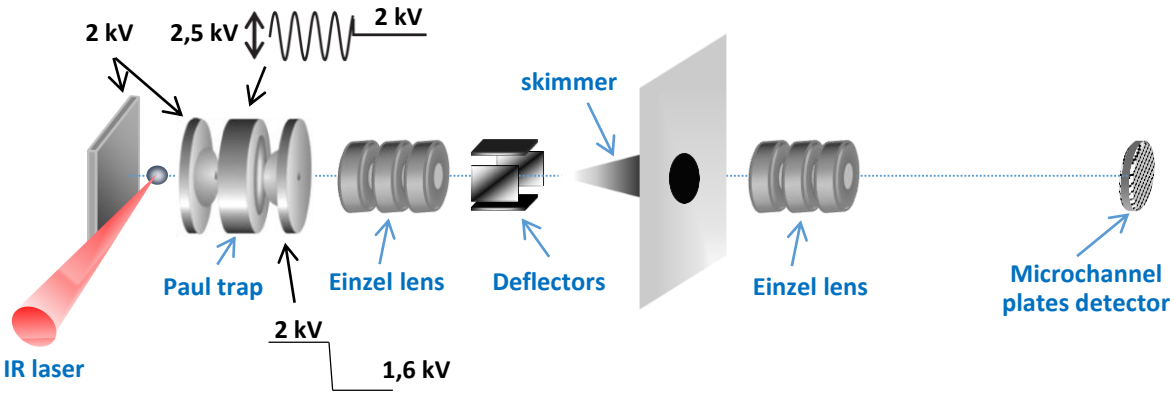

Figure 2 : Schematic view of the coupling of the IR laser desorption on microdroplets with a Paul trap. The first electrode and the entrance end cap electrode of the trap are holded at a potential of about 2 kV, with a small difference adjusted to get slow ions at the entrance of the trap. The different indicated potentials correspond to the extraction, trapping and detection of cations, but the whole set-up can work in a negative mode.

3 Results and discussion.

The stroboscopic visualization of the droplet allows to get instantaneous images at the exit of the microdrop dispenser, at the entrance of the first skimmer, just before the intermediate chamber, at the entrance of the second skimmer, just before the desorption chamber, and in the area where the droplet trajectory crosses the IR laser beam, in order to follow the shattering of the droplet. The different transit times of the droplet are given in the table III. From these transit times, it can be seen that the time spent by the droplet in the desorption chamber, where the pressure is below $9\ 10^{-6}$ mbar, is less than 3 ms. During their path, the droplets are evaporatively cooled and if they are cooled to a sufficiently low temperature they may freeze, at least on its surface. Nevertheless, the droplets can exist in the liquid state at

temperatures far below their normal melting point. For instance, tiny droplets of supercooled water at temperatures as low as 238 K naturally occur in the upper clouds of Earth's atmosphere[77]. Many recent studies were devoted to the freezing processes of liquid droplets under vacuum[78-84]. Ando and co-workers showed that a 50 micrometers droplet of ethylene glycol levitating in an ion trap survives as a liquid for more than tens of seconds due to the balance between evaporative cooling and radiative heating from the ambient room temperature[82]. The same group has also found that 49 micrometers droplets of pure water freezed at a time between 7.0 and 7.9 ms after being generated at room temperature[84], where the fraction of frozen droplets increased from 5% to 95% in 1 ms. These results suggest that our droplets, which are a mixture of water and DMSO, are in a state of supercooled liquid just before the interaction with the IR desorption laser. This is conforted by our experimental observations during the alignment of our set-up : when we place a metallic tip on the droplets trajectory, in the center of the desorption chamber, we observe the formation of a rapidly growing stalagmite on the top of this tip (up to one millimeter long), which suggests an instantaneous freezing of the droplets when they touch the tip.

Position	Pressure (mbar)	Transit time (ms)	Droplet speed ($m.s^{-1}$)
First skimmer	280	1,2	20
Second skimmer	$8\ 10^{-2}$	2,3	22
Crossing with the IR laser	$5\text{-}9\ 10^{-6}$	5,3	25

Table III : Transit times of the droplet along its trajectory. The first skimmer separates the generator chamber from the intermediate chamber. The second skimmer separates the intermediate chamber from the desorption chamber. The droplet trajectory crosses the IR laser beam at the center of the desorption chamber. The speeds are average speeds for each segment.

We use a mixture of DMSO and water in order to get a better droplet ejection stability. As already stated, the microdrop dispenser is housed in a pumped chamber (280 mbar), which does not correspond to its normal operation. The DMSO is an organic solvent whose vapour pressure (0.6 mbar at room temperature) is much lower than the one of water (23 mbar at room temperature), and whose dynamical viscosity ($2\ 10^{-3}$ Pa.s at room temperature) is higher than the one of water (10^{-3} Pa.s at room temperature). These two characteristics facilitate the formation and the ejection of the droplets when the voltage pulse is applied to the piezoelectric generator. The DMSO also presents a strong absorption band at 3.3 µm and is

then well adapted to the IR desorption of the droplets. The limit of stability for droplet ejection with our experimental parameters corresponds to a mixture of 1/4 DMSO with 3/4 water, but it is possible to work for short times with water only droplets. Once the droplet arrives at the center of the generator chamber, an IR laser pulse is sent to irradiate them. A triggered light emitting diode (LED) and a magnification optical

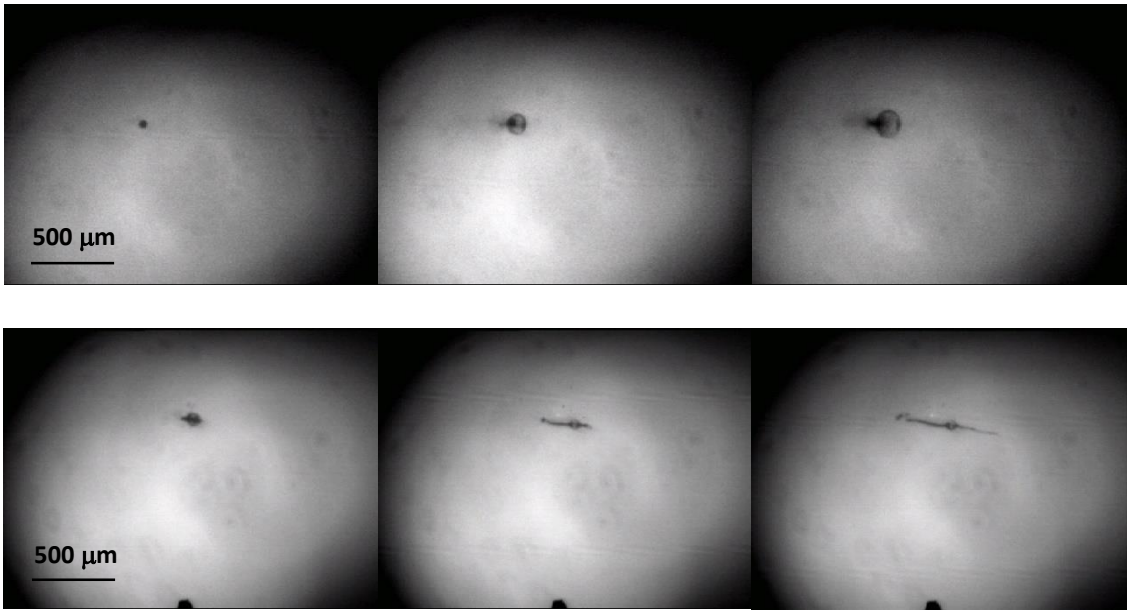

Figure 3 : Images of the microdroplet while interaction with the desorption laser takes place. For the top snapshots sequence, the delay between the laser impulsion and the image capture is, from left to right : Δt = 0 μs, Δt = 2 μs and Δt = 20 μs. For the bottom snapshots sequence, these delays are Δt = 1 μs, Δt = 3 μs and Δt = 20 μs The two sequences correspond to two different wavelenghts and then to two different penetration depths and two ejection mechanisms. The top sequence corresponds to a more or less isotropic expansion of the droplet in the plane perpendicular to the laser beam, while the bottom sequence corresponds to an anisotrope shattering of the droplet into many pieces of small fragments.

system situated inside the desorption chamber allow to visualize the droplet expansion and shattering which takes place during a few tens of microseconds after the laser pulse. There are little position fluctuations of the droplets (the position of the droplets is the same within 100 μm after a 10 cm flight, and the instant at which the droplet crosses the laser beam trajectory is the same within 2 μs at each period), and almost all IR laser pulses aimed at the incoming droplets hit them. Depending on several experimental parameters (energy of the laser pulse, wavelength, position of the droplet as compared with the focus point of the

beam), different phenomena are observed. For high energy laser pulses (5 mJ, which corresponds to 125 MW.cm^{-2}) and wavelengths off-tuned to the OH strectching mode of water and to the CH stretching mode of DMSO, laser induced plasma[85,86] are observed. These experimental conditions lead to very energetic product particles, almost insensitive to the acceleration field, arriving on the microchannel plate detector in less than 1 μs and producing a very intense signal. For lower energy laser pulses, two different behaviours are observed depending on the wavelength (see Figure 3) : for small laser light penetration depth (wavelength resonant with an absorption band of the solvent), the droplet is disintegrated in a pattern having a completly anisotropic structure, while for a longer penetration depth (wavelength slightly detuned to the red as compared with the absorption band of the solvent), the expansion of the droplet is more or less isotropic in the plane perpendicular to the laser beam. Such a dependency of the disintegration process with the wavelength of the laser beam was nicely observed by Stasicki and co-workers for a liquid jet by means of high-speed video stroboscopy[66]. The two different behaviours were associated with a non-thermal (shock wave) and a thermal process, and the shock wave propagation, predicted by MD simulations of surface impact of rare-gas clusters was also observed by Terasaki using a pump-probe technique[68]. The isotropic expansion of the droplet leads to product ions which we extract with acceleration fields, while we did not get any signal with the anisotropic disintegration. All the spectra presented below are then obtained with a setting of the laser wavelength associated with the isotropic expansion.

Figure 4 shows a spectrum obtained in the positive mode for a nonapeptide, bradykinin (m = 1060 Da). Protonated bradykinin is clearly observed together with solvent clusters ($H_3O^+(DMSO)_n$, with n=3-6). Such clusters have already been evidenced in investigations on the microheterogeneity of the water-DMSO solvent mixture[87]. Bradykinin ions are only observed in a singly charge state while bradykinin has two basic arginin residues. According to Brutschy and co-workers, the predominance of low charge states for desorbed ions is the hint of strong ion recombination and thus charge neutralization during the desorption process[40]. This ion-ion recombination has been identified by Baer and co-workers[88] as the major cause of signal saturation with concentration after IR vaporization of ethylene-glycol droplets (2-5 μm). We can also observe that there is no fragmentation of bradykinin.

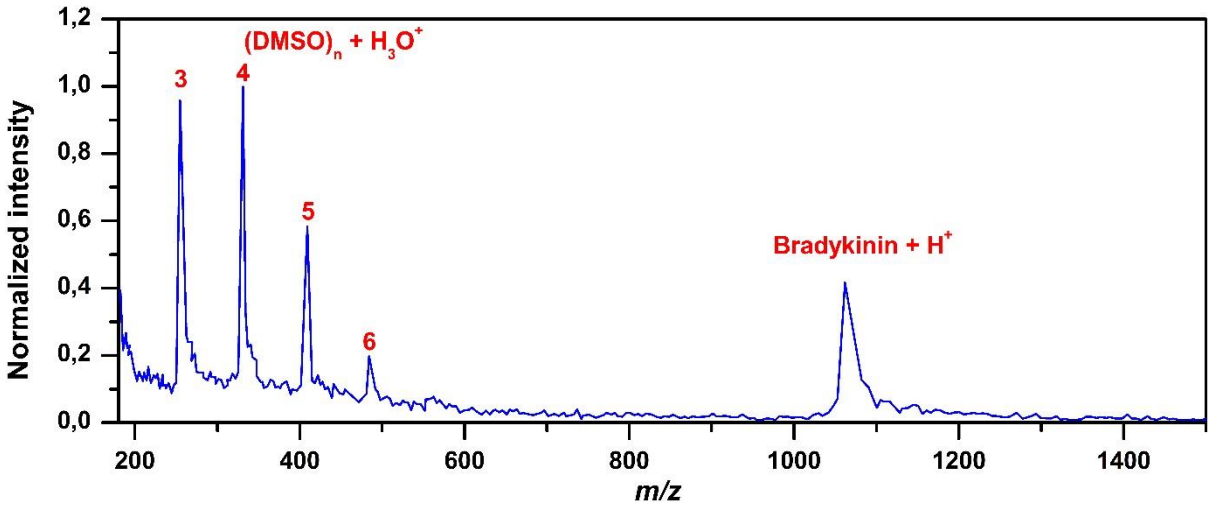

Figure 4 : Mass spectrum of product ions obtained by IR laser desorption of microdroplets of a mixture of DMSO and H_2O (3/4 - 1/4) with Bradykinin at a concentration of 100 µmol.L^{-1} for a laser pulse energy of 3 mJ and an extraction delay of 7 µs. The extraction line is set in a positive mode.

This spectrum presents a mass resolution of about 85 at *m/z* = 1000. This rather low mass resolution is attributed to the very broad velocity distribution resulting from the IR laser desorption. Velocities in the range 5000-8000 m.s^{-1} have been measured by Abel and co-workers for laser induced liquid water jet desintegration[66], and Terasaki has measured velocities in the range 700-1300 m.s^{-1} for molecules ejected from ethanol droplets irradiated by a 8 mJ IR laser[68]. Kohno and co-workers have evidenced fast (1400-2300 m.s^{-1}) and slow (780-1500 m.s^{-1}) components in the ejection of hydrated aniline clusters after irradiation of a liquid beam by an IR laser in the energy range 0,5-8 mJ[70].

Pulsed ion extraction acts as an ion gate for this incoming broad translationnal energy distribution of the ionic species and then improves mass resolution. As can be seen on top of Figure 5, when the desorption is realized directly in the extraction area, the mass resolution falls down to 18.

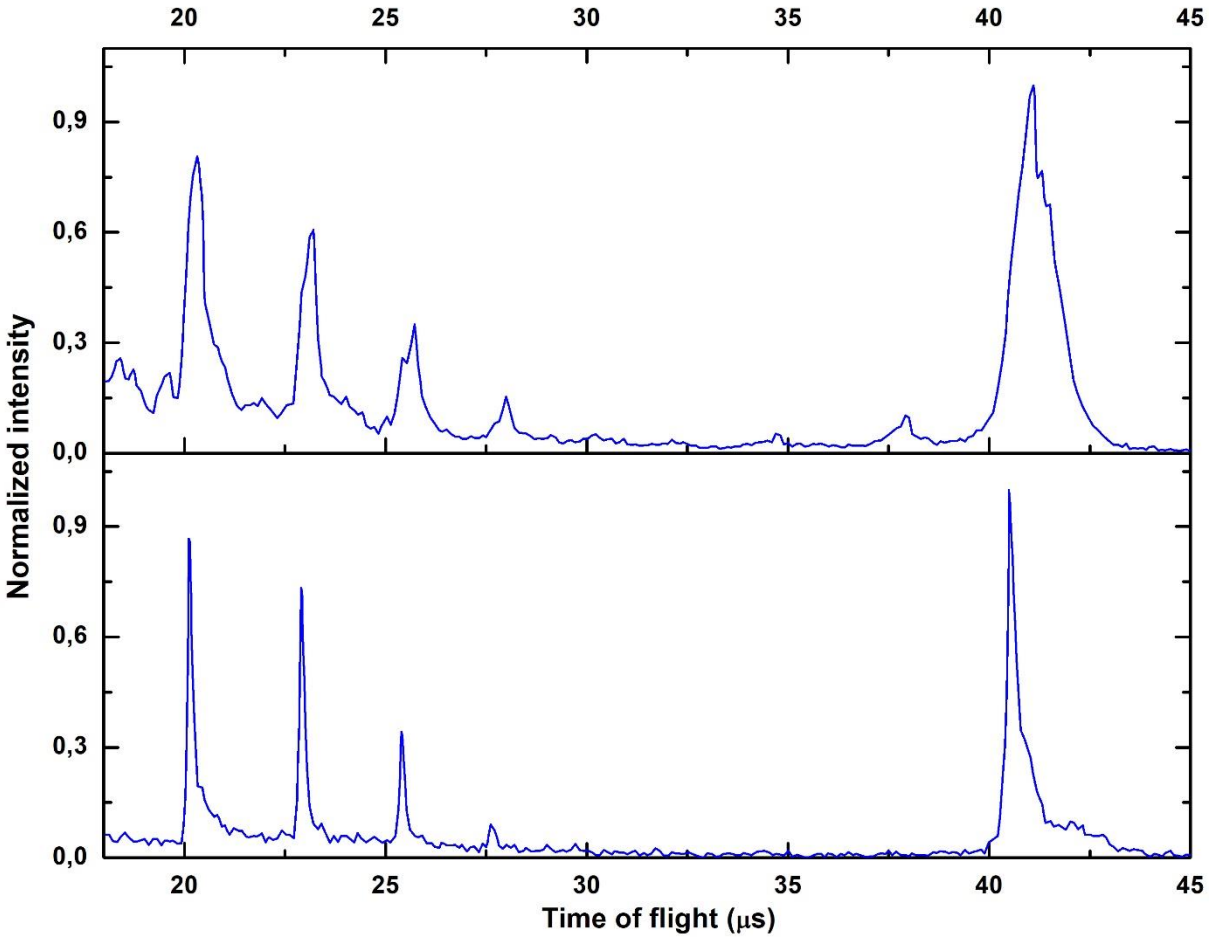

Figure 5 : Effect of the pulsed ion extraction on the mass resolution for mass spectra of products ions obtained by IR laser desorption of microdroplets of a mixture of DMSO and H_2O (3/4-1/4) with Bradykinin at a concentration of 100 µmol.L^{-1} for a laser pulse energy of 3 mJ. Top : the desorption is realized directly in the extraction area. The mass resolution is about 18 at m = 1000 Da (41 µs). Down : pulsed ion extraction (time delay of 7 µs between the laser pulse and the pulsed accelerating field). The mass resolution is about 85 at m = 1000 Da.

As no active charging occurs in the LILBID process, anionic and cationic charged species can be released from the droplet at the same time. Figure 6 shows mass spectra in the positive and in the negative modes obtained by IR laser ablation of microdroplets of a mixture of DMSO and H_2O (3/4 - 1/4) containing different biomolecules whose masses are in the range 1000-2000 Da. On the bottom of Figure 6, the droplets contain a mixture of bradykinin with Tryptophan zipper TZ4 (m = 2012 Da), a monomeric beta-hairpin constituted of 16 amino-acids[89]. With an extraction delay of 9 µs in the positive mode, the singly protonated bradikynin ion signal is optimized, and we can also detect ions corresponding to singly protonated TZ4. The top of Figure 6 corresponds to droplets containing bradykinin and vancomycin (m = 1449

Da), and in the negative mode the singly deprotonated bradykinin signal has about the same intensity as the one of protonated bradykinin in the positive mode.

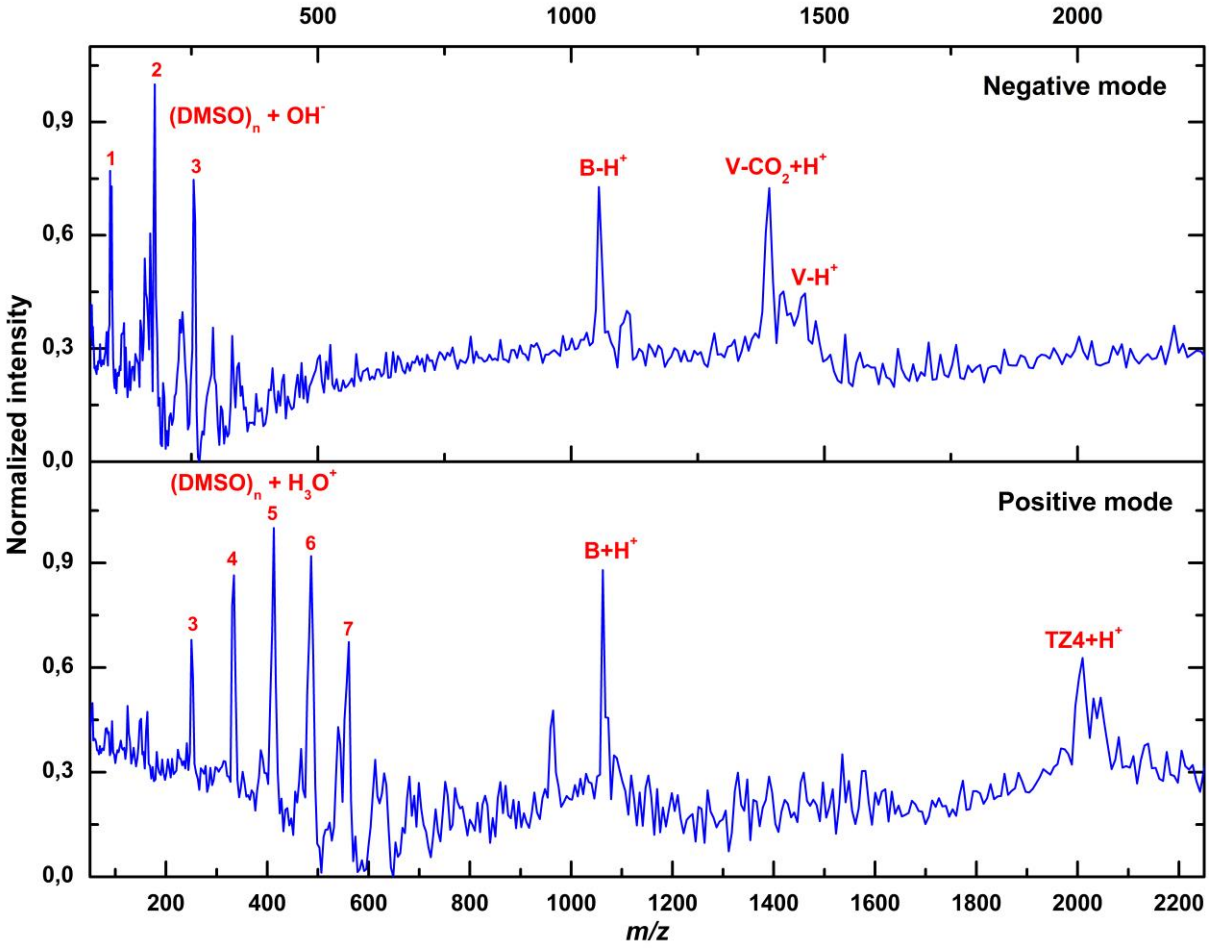

Figure 6 : Mass spectrum of product ions obtained by IR laser desorption of microdroplets of a mixture of DMSO and H_2O (3/4 - 1/4) and for a laser pulse energy of 3 mJ. Bottom : Bradykinin (B) and Tryptophan Zipper TZ4 (at an equal concentration of 10 µmol.L^{-1}) in a positive mode and for an extraction delay of 9 µs. Top : Bradykinin (B) and Vancomycin (V) (at an equal concentration of 100 µmol.L^{-1}) in a negative mode and for an extraction delay of 7 µs.

As can be seen in the spectrum on top of figure 6, some fragmentation is observed for vancomycin. Even if the singly deprotonated vancomycin ions are observed, fragmentation with the loss of CO_2 is predominant. This loss of the carboxylic group from the dihydroxyphenylglycine residue corresponds to the main abundant product observed at low energy in the CID spectrum of vancomycin[90,91], which makes of vancomycin a very sensible test molecule for the study of the softness of our source. In this perspective, we have studied the influence of the laser energy pulse on the intensity of the product ions and on the

decarboxylation of vancomycin. Figure 7 shows the evolution of the signal as a funtion of the laser energy pulse for the IR laser desorption of microdroplets of DMSO with vancomycin at a concentration of 10^{-4} M, for an extraction delay of 8 μs, in the negative mode. We observe the appearance of a signal for vancomycin at a threshold laser energy of 1.5 mJ. At this energy, only few fragmentation occurs. For an energy pulse of 2 mJ, the intensity of the peak associated with vancomycin grows significantly, but fragmentation of vancomycin during the desorption process also becomes more important.

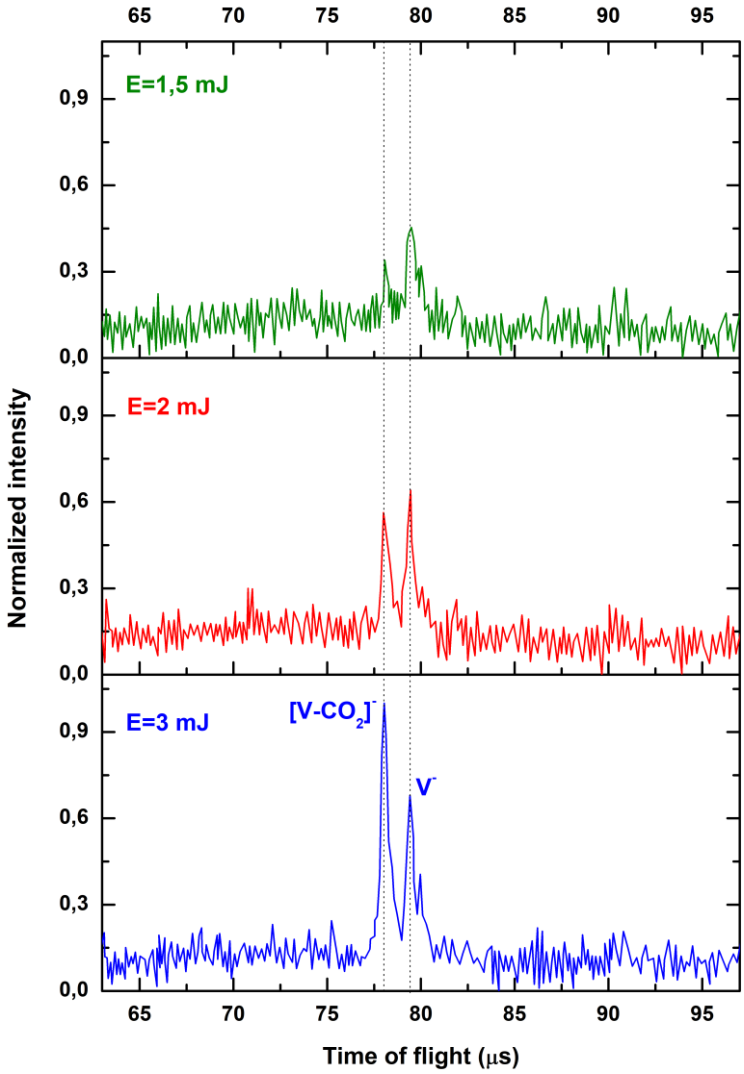

Figure 7 : Time of flight of product ions obtained by IR laser desorption of microdroplets of DMSO with Vancomycin (100 μmol.L^{-1}) for a same wavelength but for different laser pulse energies. The extraction line is set in a negative mode and the extraction delay is set to 8 μs.

For an energy pulse of 3 mJ, the intensity of the peak associated with vancomycin has only slightly grown, but fragmentation with the loss of CO_2 is now predominant. The optimal energy pulse allowing to get the higher signal with the lower fragmentation is then just below 3 mJ. For such an energy, Figure 8 shows the influence of the extraction delay on the detected signal for the IR laser desorption of microdroplets of H_2O with vancomycin at a concentration of 10^{-4} M. For a delay of 1 µs, the detected species correspond to negatively charged small agregates of H_2O. For longer delays, species with higher *m/z* are detected : the pulsed ion optics acts as an ion gate. For a delay of 7 µs, deprotonated vancomycin is detected along with V $(H_2O)_n$ complexes , then at 10 µs dimer of vancomycin and at 13 µs trimer of vancomycin. After 15 to 20 µs, we do not detect any more ion signal. As can be seen on these spectra, there is only few fragmentation, and the detected ions are only once deprotonated while vancomycin contains two carboxylic acid groups which are susceptible to lose a proton.

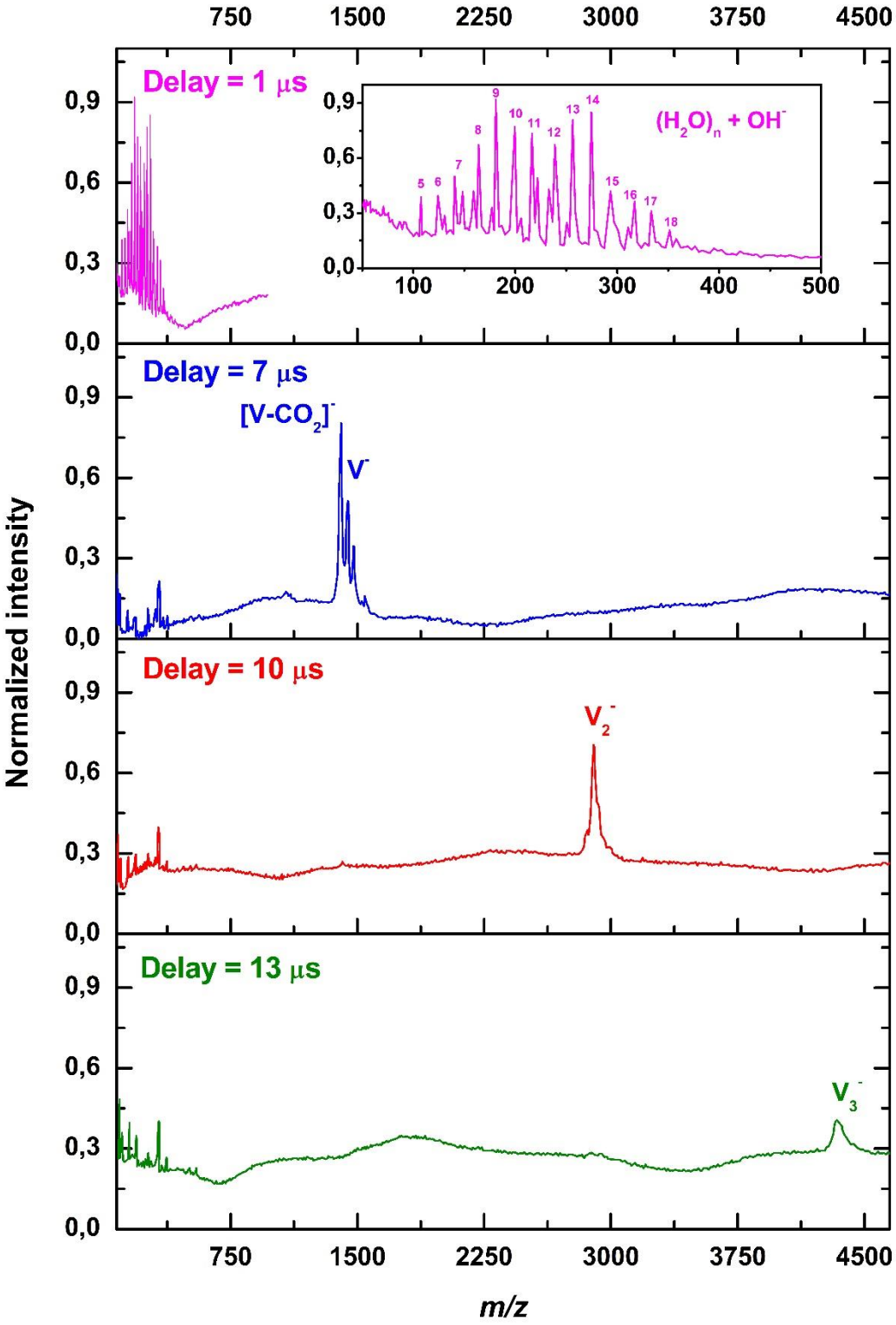

Figure 8 : Time of flight of product ions obtained by IR laser desorption of microdroplets of H_2O with Vancomycin (100 µmol.L^{-1}) for a laser pulse energy of 3 mJ and for different time delays between laser pulse and ion extraction. V^- stands for deprotonated vancomycin, V_2^- for the deprotonated dimer of vancomycin and V_3^- for the deprotonated trimer of vancomycin. The inset on the top figure corresponds to a zoom in the 50-500 u mass range.

We have also performed the IR laser desorption of microdroplets of DMSO with vancomycin and the caped tripeptide N^{α},N^{ε}-diacetyl-L-Lys-D-Ala-D-Ala (Ac_2KAA, m=372 Da) at a concentration of 10^{-4} M (Figure 6). The KAA terminal peptidic sequence of Lipid II, a precursor of peptidoglycans, is enantiospecifically recognized by vancomycin[92,93], and we have previously shown that the native structure of the deprotonated vancomycin-$Ac_2{}^{L}K^{D}A^{D}A$ non-covalent complex was preserved in the gas phase[94] while none of the native interactions are preserved for the doubly protonated species obtained by ESI[95]. The gas phase desorption of this complex by IR desorption from microdroplets would then be a first step towards the further study of its structure in order to compare it with the one resulting from ESI. As can be seen on Figure 9, the vancomycin-$Ac_2{}^{L}K^{D}A^{D}A$ non-covalent complex is preserved in the gas phase, which is in concordance with the soft desorption described previously for LILBID (even if it might be underlined that this complex is obtained by ESI, which is a sign of the high affinity of the tripeptide with vancomycin). It can also be underlined that this complex, as well as vancomycin alone or Ac_2KAA alone, are observed in low charge states (the different peaks correspond to once deprotonated species), which is a general characteristic of LILBID[35,45] and MALDI in general.

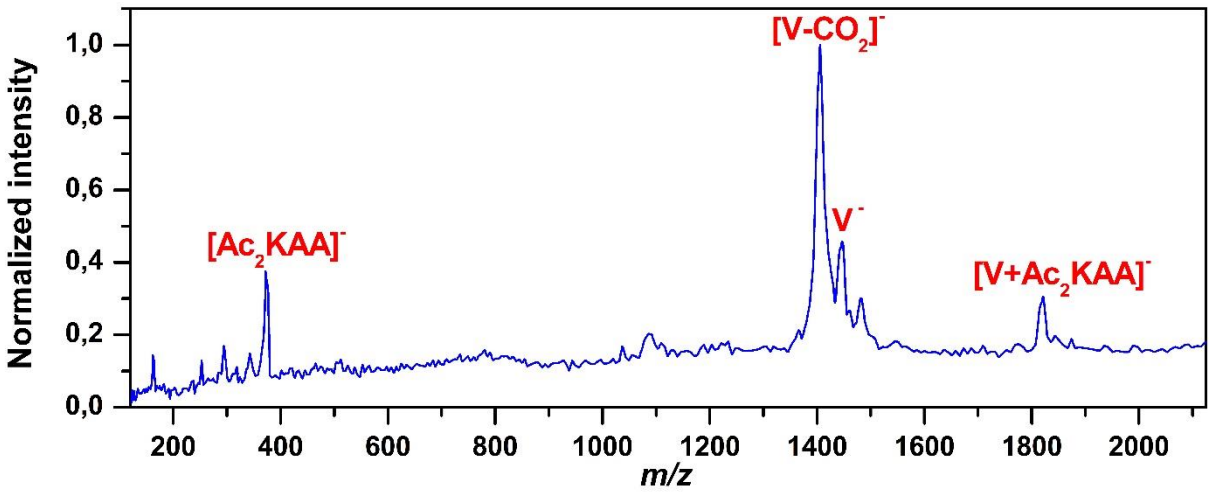

Figure 9 : Mass spectrum of product ions obtained by IR laser desorption of microdroplets of a mixture of DMSO and H_2O (3/4-1/4) with Vancomycin (V) and the caped tripeptide N^{α},N^{ε}-diacetyl-L-Lys-D-Ala-D-Ala (Ac_2KAA) (at an equal concentration of 100 µmol.L^{-1}) for a laser pulse energy of 3 mJ and an extraction delay of 8 µs. The extraction line is set in a negative mode.

Pulsed ion extraction improves partially this resolution but does not allow to completly compensate for the very broad initial conditions. To get insight into the ability of our pulsed ion extraction to improve mass resolution, we have made a simulation with SIMION[96] of the delayed extraction line and we have compared the simulated time of flights with the experimental ones. Figure 10 shows such a comparison in the case of the IR laser ablation of DMSO microdroplets containing the Ac_2KAA tripeptide with vancomycin. The experimental conditions were chosen in order to increase the signal on the mass of the tripeptide (m = 372 Da) while getting a sufficiently high signal for the identification of vancomycin (m = 1449 Da) and of the complex formed between vancomycin and the tripeptide (m = 1821 Da).

In the simulation, ions were generated with a very broad translational energy distribution of 100 eV, which corresponds to velocities in the range 0-7200 $m.s^{-1}$ for the tripeptide and 0-3200 $m.s^{-1}$ for the complex. Such velocity distributions are in agreement with the experimental results reported above. The different positions of electrodes and applied potentials are reported in Table III. The time delay between the pulsed accelerating field and the ion creation time was set to the same value (9 µs) as the time delay between the pulsed accelerating field and the laser pulse since the ion ejection process happens on a much smaller time scale. The pulsed accelerating field duration is 1 µs. With these conditions, the arrival times on the microchannel plates detector are represented on Figure 10 b.

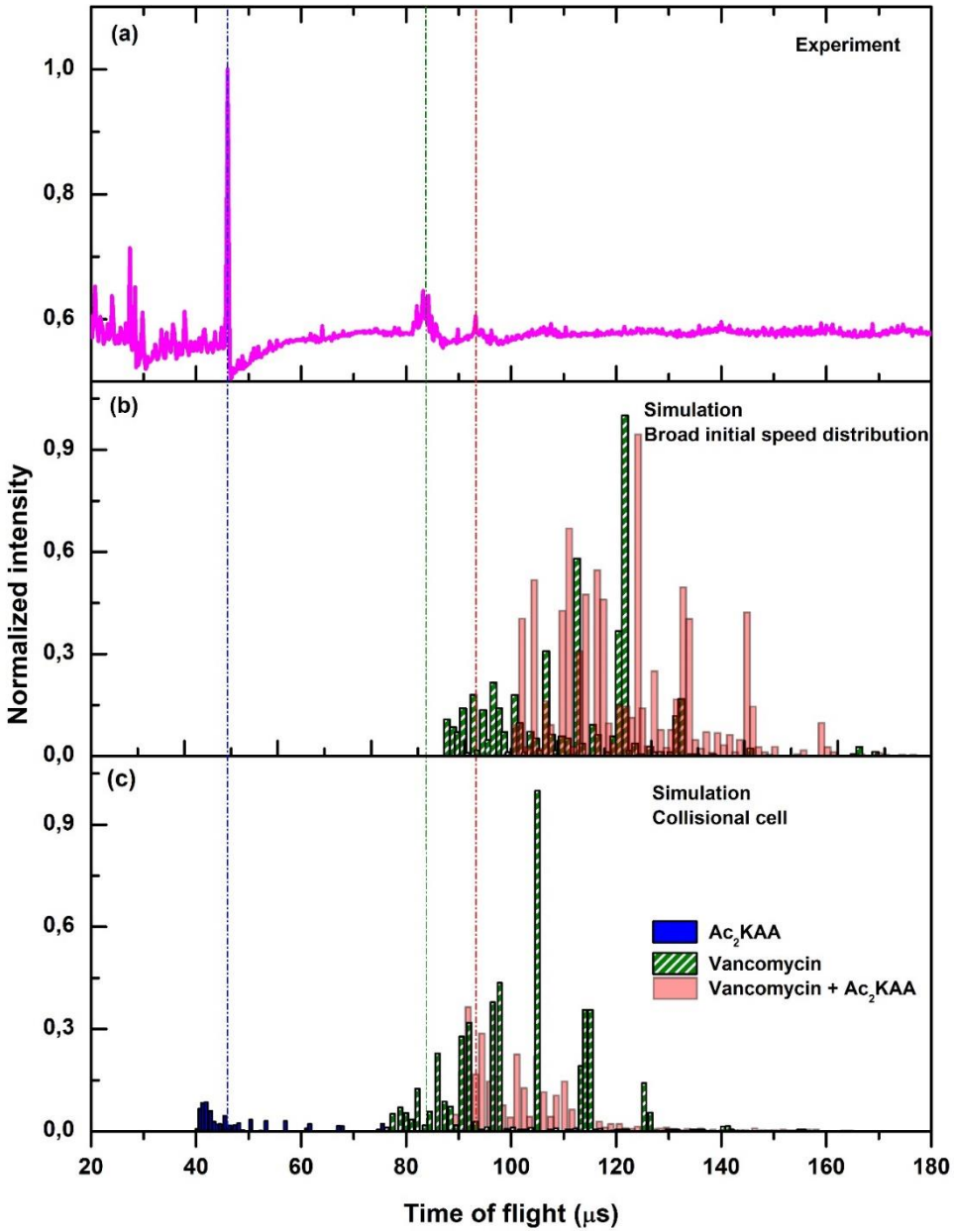

Figure 10 : Comparison between a time of flight spectrum obtained by IR laser desorption of microdroplets and simulations of the ions trajectories realized with Simion. (a) : Time of flight spectrum of product ions obtained by IR laser desorption of microdroplets of a mixture of DMSO and H_2O (3/4-1/4) with Vancomycin (V) and the caped tripeptide N^{α},N^{ε}-diacetyl-L-Lys-D-Ala-D-Ala (Ac_2KAA) (at an equal concentration of 100 μmol.L^{-1}) for a laser pulse energy of 3 mJ and an extraction delay of 9 μs. (b) : Simulation by SIMION of the ions arriving on the microchannel plates detector for a large dispersion of the initial speeds (0-3250 m.s^{-1}). (c) : Same as (b) but with the adding of a collisional cell in the ion creation area, and an energy cutoff of the detector.

These distributions for vancomycin and for the complex are much broader than the experimental ones. Surprisingly, no tripeptide ion reaches the detector in the simulation while the experimental parameters were set in order to optimize this signal. Adjusting the duration time of the pulsed ion optics, in order to take into account electronic times for the rise-up and

the fall down of the accelerating field, does not change significantly the simulated arrival times, neither adjusting slightly the delay time between the ion creation time and the pulsed accelerating field. In all cases, tripeptide ions are too fast and have already traveled through the pulsed extraction area before the pulsed accelerating field is applied. They do not get a sufficient energy to overpass the potential barrier of the first Einzel lens. The experimental spectrum indicates clearly that these ions arrive in the extraction area later than predicted by these SIMION simulations. Such simulations realized under vacuum are certainly not representative of the first tens of micrometers traveled by the ejected ions. As can be seen on the snapshots of the droplet explosion on Figure 3, a dense environment is observed during several microseconds after the laser pulse. To take into account these initial conditions, we have added in our simulations a cubic collision cell centered on the ion creation zone and whose side is 250 µm long. The cell was filled with particles whose mass was chosen to be the mass of water. Collisions with these particles slow down the ejected ions, and we have adjusted the average free path in the cell so that tripeptide ions arrived at the experimental time. This adjustment leads to an average free path of 10 µm, which corresponds to an average pressure of 25 mbar for water molecules with a 2 Å diameter at an ambient temperature. With this coarse model, simulations predict arrival times for the three species of interest (tripeptide, vancomycin and the complex) which are in agreement with the experimental spectrum (Figure 10c), even if the simulated arrival time distributions are still larger than the experimental ones.

Even with a pulsed ion extraction, the broad velocity distribution of the ejected ions limits the mass resolution and then the identification of the desorbed species. To overcome this limitation, different experimental strategies have been proposed. Sugiyama and co-workers have proposed a dual laser shattering of the microdroplets[97] which implies a spatial compression of the splashes and can enhance the efficiency of ion formation with a lower dispersion velocity. Kohno and co-workers have realized the IR ablation of microdroplets in an ion trap[72] so that the product ions are readily trapped with high efficiency. We propose here a different coupling of our IR laser desorption source with an ion trap : as described in section 2, the IR laser ablation takes place at the entrance (and not inside) an ion trap. The droplet is irradiated a few millimeters upstream the entrance endcap electrode of a Paul Trap and a low accelerating field (a few volts per centimeter) drives the ejected ions inside the trap. The local

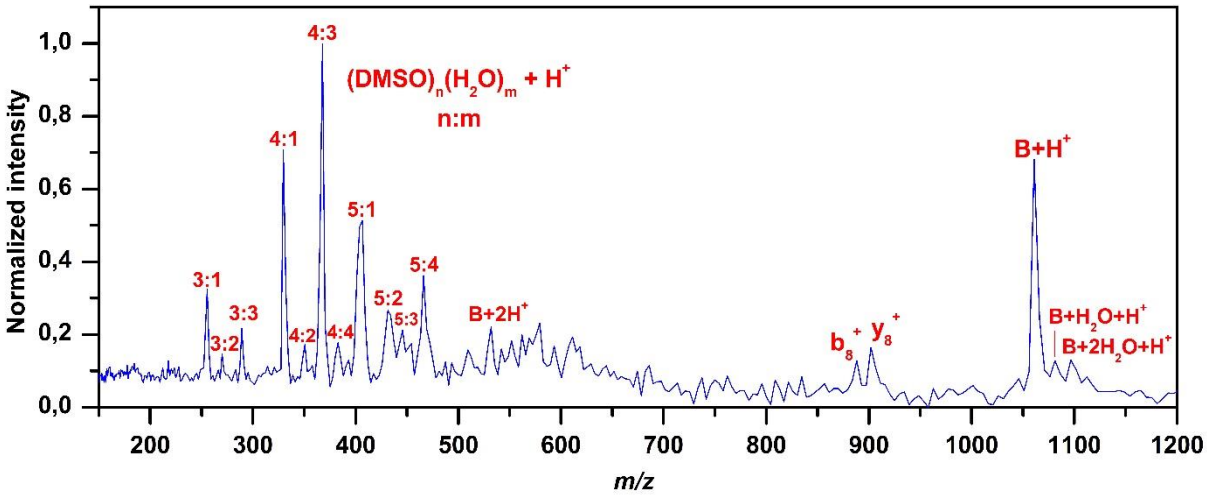

Figure 11 : Mass spectrum of product ions obtained by IR laser desorption of microdroplets of a mixture of DMSO and H_2O (3/4 - 1/4) with Bradykinin at a concentration of 10 µmol.L^{-1}, for a laser pulse energy of 3 mJ. The product ions are trapped during 10 ms before being mass analysed. B stands for Bradykinin.

increase of pressure, linked to the droplet ablation, conjugated with the helium injected inside the trap, implies an operation of the trap at its upper pressure limit, but we have trapped ejected ions during several milliseconds. The extraction from the trap and further acceleration of the ions is realized by biasing the whole trap to a high potential. In these conditions, we have mass analysed ions obtained by IR laser ablation of droplets containing bradykinin at a concentration of 10 µM (Figure 11). A clear increase of the mass resolution (235 at m = 1000 Da) is obtained. Hydrated complexes are observed, but we cannot ascertain whether they are preserved from the native phase or created inside the trap. The different protonated $(DMSO)_n(H_2O)_m$ clusters which are observed are constituted of a more important number of water molecules than when the trap is not used, which could tend to indicate that hydration occurs inside the trap. Unlike spectra obtained with the delayed extraction scheme, some fragmentation of bradykinin slightly occurs: y_8^+ and b_8^+ ions, corresponding to the loss of the C-terminal or N-terminal Arginin, are observed. These two ions are among the main fragments observed in CID spectra of bradykinin[98]. This reflects the difficulty to trap ions with broad velocity distributions while conserving soft collisions with the buffer gas at the entrance of the trap.

4 Conclusion.

Biomolecular ions are isolated in the gas phase by IR laser ablation of liquid microdroplets directly under vacuum. These ions are mass analysed either by a delayed extraction line or by coupling of the source with an ion trap. The setup displays comparable efficiencies in the positive and in the negative mode, allows to get low charge states in the gas phase, presents weak fragmentation during the desorption process and allows to conserve complexes in the gas phase. The first results of the coupling of the desorption source with a Paul trap prove the feasibility of this coupling and confirm the expected increase of the mass resolution. This new experimental strategy opens a promising way to take advantage of the soft LILBID desorption to analyse the structure of small biomolecules by means of action spectroscopy.

References.

(1) Johnstone R.A.W.; Rose M.E. Macrocyclic ligands examined by fast atom bombardment mass spectrometry : direct observation of metal cation selectivity in complexation. *J. Chem. Soc., Chem. Commun.* **1983**, 21, 1268-1270.

(2) Michaud D.P.; Kyranos J.N.; Brennan T.F.; Vouros P. Examination of ligand-ligand interactions by fast atom bombardment mass spectrometry. *Anal. Chem.* **1990**, 62,10, 1069-1074.

(3) Yamashita M. ; Fenn J.B. Electrospray ion source. Another variation on the free-jet theme. *J. Phys. Chem.* **1984,** *88*, 4451-4459.

(4) Fenn J.B. ; Mann M.; Meng C.K.; Wong S.F.; Whitehouse C.M. Electrospray ionization for mass spectrometry of large biomolecules. *Science* **1989,** *246*, 64-71.

(5) Karas M. ; Bachmann D. ; Bahr U. ; Hillenkamp F. Matrix-assisted ultraviolet laser desorption of nonvolatile compounds. *Int. J. Mass Spectrom.* **1987**, *78*, 53-68.

(6) Karas M. ; Hillenkamp F. Laser desorption ionization of proteins with molecular masses exceeding 10,000 Daltons. *Anal. Chem.* **1988**, *60 (20)*, 2299-2301.

(7) Hernández H. ; Robinson C.V. ; Determining the stoichiometry and interactions of macromolecular assemblies from mass spectrometry. *Nat. Protoc.* **2007**, *2*, 715-726.

(8) Heck A.J. ; Native mass spectrometry : a bridge between interactomics and structural biology. *Nat. Meth.* **2008**, *5*, 927-933.

(9) Barrera N.P. ; Isaacson S.C. ; Zhou M. ; Bavro V.N. ; Welch A. ; Schaedler T.A. ; Seeger M.A. ; Miguel R.N. ; Korkhov V.M. ; van Veen H.W. ; Venter H. ; Walmsley A.R. ; Tate C.G. ; Robinson C.V. Mass spectrometry of membrane transporters reveals subunit stoichiometry and interactions. *Nat. Meth.* **2009**, *6*, 585-587.

(10) Uetrecht C. ; Rose R.J. ; van Duijn E. ; Lorenzen K. ; Heck A.J. Ion mobility mass spectrometry of proteins and proteins assemblies. *Chem. Soc. Rev.* **2010**, *39*, 1633-1655.

(11) Barrera N.P. ; Robinson C.V. Advances in the mass spectrometry of membrane proteins : from individual proteins to intact complexes. *Annu. Rev. Biochem.* **2011**, *80*, 247-271.

(12) Marcoux J. ; Robinson C.V. ; Twenty years of gas phase structural biology. *Structure*. **2013**, *21*, 1541-1550.

(13) Chen F. ; Gülbakan B. ; Weidmann S. ; Fagerer S.R. ; Ibáñez A.J. ; Zenobi R. Applying mass spectrometry to study non-covalent biomolecule complexes. *Mass Spectrom. Rev.* **2016**, *35*, 48-70.

(14) Wortmann A. ; Pimenova T. ; Alves S. ; Zenobi R. Investigation of the first shot phenomenon in MALDI mass spectrometry of protein complexes. *Analyst*. **2007**, *132*, 199-207.

(15) Wang Z. ; Yu X. ; Cui M. ; Liu Z. Investigation of calmodulin-peptide interactions using matrix-assisted laser desoprtion/ionization mass spectrometry. *J. Am. Soc. Mass Spectrom.* **2009**, *20*, 576-583.

(16) Zehl M. ; Allmaier G. Instrumental parameters in the MALDI-TOF mass spectrometric analysis of quaternary protein structures. *Anal. Chem.* **2005**, *77*, 103-110.

(17) Van Duijn E.; Current limitations in native mass spectrometry based structural biology. *J. Am. Mass Spectrom.* **2010**, *21*, 971-978.

(18) Breuker K. ; McLafferty F.W. Stepwise evolution of protein native structure with electrospray into the gas phase, 10^{-12} to 10^{2} s. *Proc. Natl. Acad. Sci.* **2008,** *105 (47),* 18145-18152.

(19) Leitner A. ; Walzthoeni T. ; Kahraman A. ; Herzog F. ; Rinner O. ; Beck M. ; Aebersold R. Probing native protein structures by chemical cross-linking mass spectrometry, and bioinformatics. *Mol. Cell Proteomics* **2010**, *9*, 1634-1649.

(20) Müller M.Q. ; Sinz A. Chemical cross-linking and high-resolution mass spectrometry to study protein-drug interactions. *Meth. Mol. Biol.* **2012**, *803*, 205-218.

(21) Becker C.H.; Jusinski L.E.; Moro L. Infrared laser-induced desorption of neutral organic compounds from frozen aqueous solution followed by single-photon ionization. *Int. J. Mass Spectrom. Ion Processes* **1990**, 95, R1-R4.

(22) Berkenkamp S.; Karas M.; Hillenkamp F. Ice as a matrix for IR-matrix-assisted laser desorption/ionization : mass spectra from a protein single crystal. *Proc. Natl. Acad. Sci. USA* **1996**, 93, 7003-7007.

(23) Murray K.K.; Sheffer J.D. Infrared matrix-assisted laser desorption/ionization using a frozen alcohol matrix. *J. Mass Spectrom.* **2000**, 35, 95-97.

(24) Siegbahn H.; Siegbahn K. ESCA applied to liquids. *J. Electron Spectry* **1973**, 2, 319-325.

(25) Keller W.; Morgner H.; Müller W.A. Electron spectroscopy of liquid mercury under impact of metastable He(2^{3}S) atoms. *Mol. Phys.* **1986**, 58, 6, 1039-1052.

(26) Faubel M.; Schlemmer S.; Toennies J.P. A molecular beam study of the evaporation of water from a liquid jet. *Z. Phys. Chem.* **1988**, 10, 269-277.

(27) Faubel M.; Kisters T. Non-equilibrium molecular evaporation of carboxylic acid dimers. *Nature* **1989**, 339, 527-529.

(28) Nishi N.; Koga K.; Ohshima C.; Yamamoto K.; Nagashima U.; Nagami J. Molecular association in ethanol-water mixtures studied by mass spectrometric analysis of clusters generated through adiabatic expansion of liquid jets. *J. Am. Chem. Soc.* **1988**, 110, 5246-5255.

(29) Yamamoto K.; Nishi N. Hydrophobic hydration and hydrophobic interaction of carboxylic acids in aqueous solution : mass spectrometric analysis of liquid fragments isolated as clusters. *J. Am. Soc.* **1990**, 112, 549-558.

(30) Mafuné F.; Takeda Y.; Nagata T.; Kondow T. Formation and ejection of cluster ions from a liquid beam of aniline-ethanol solution by laser photoionization. *Chem. Phys. Lett.* **1992**, 199, 615-620.

(31) Horimoto N.; Kohno J.-Y.; Mafuné F.; Kondow T. Preparation of less volatile solute molecules and clusters in the gas phase through selective vibrational excitation of solvent in liquid beam of solution. *J. Phys. Chem. A* **1999**, 103, 9569-9572.

(32) Kondow T.; Mafuné F. Structures and dynamics of molecules on liquid beam surfaces. *Annu. Rev. Phys. Chem.* **2000**, 51, 731-761.

(33) Kleinekofort W. ; Avdiev J. ; Brutschy B. A new method of laser desorption mass spectrometry for the study of biological macromolecules. *Int. J. Mass Spectrom. Ion Processes* **1996,** *152,* 135-142.

(34) Kleinekofort W.; Pfenninger A.; Plomer T.; Griesinger C.; Brutschy B. Observation of noncovalent complexes using laser-induced liquid beam ionization/desorption. *Int. J. Mass Spectrom. Ion Processes* **1996**, 156, 195-202.

(35) Charvat A.; Abel B. How to make big molecules fly out of liquid water : applications, features and physics of laser assisted liquid phase dispersion mass spectrometry. *Phys. Chem. Chem. Phys.* **2007**, 9, 3335-3360.

(36) Sobott F.; Kleinekofort W.; Brutschy B. Cation selectivity of natural and synthetic ionophores probed with laser-induced liquid beam mass spectrometry. *Anal. Chem*. **1997**, 69, 3587-3594.

(37) Wattenberg A.; Barth H.-D.; Brutschy B. Copper-binding abilities of the tripeptide diglycylhistidine studied by laser-induced liquid beam ionization/desorption mass spectrometry in aqueous solution. *J. Mass Spectrom.* **1997**, 32, 1350-1355.

(38) Kleinekofort W.; Schweitzer M.; Engels J.W.; Brutschy B. Analysis of double-stranded oligonucleotides by laser-induced liquid beam mass spectrometry. *Int. J. Mass Spectrom. Ion Proc.* **1997**, 163, 1L-4L.

(39) Sobott F.; Wattenberg A.; Barth H.-D.; Brutschy B. Ionic clathrates from aqueous solutions detected with laser induced liquid beam ionization/desorption mass spectrometry. *Int. J. Mass Spectrom.* **1999**, 185/186/187, 271-279.

(40) Wattenberg A.; Sobott F.; Barth H.-D.; Brutschy B. Studying noncovalent protein complexes in aqueous solution with laser desorption mass spectrometry. *Int. J. Mass Spectrom.* **2000**, 203, 49-57.

(41) Charvat A.; Lugovoj E.; Faubel M.; Abel B. Analytical laser induced liquid beam desorption mass spectrometry of protonated amino acids and their non-covalently bound aggregates. *Eur. Phys. J. D* **2002**, 20, 573-582.

(42) Otten D.E.; Trevitt A.J.; Nichols B.D.; Metha G.F.; Buntine M.A. Infrared laser desorption of hydroquinone from a water-ethanol liquid beam. *J. Phys. Chem. A* **2003**, 107, 6130-6135.

(43) Charvat A. ; Lugovoj E. ; Faubel M. ; Abel B. New design for a time-of-flight mass spectrometer with a liquid beam laser desorption ion source for the analysis of biomolecules. *Rev. Sci. Instr.* **2004,** *75 (5)*, 1209-1218.

(44) Abel B. ; Charvat A. ; Diederichsen U. ; Faubel M. ; Girmann B. ; Niemeyer J. ; Zeeck A. Applications, features, and mechanistic aspects of liquid water beam desorption mass spectrometry. *Int. J. Mass Spectrom.* **2005,** *243*, 177-188.

(45) Morgner N. ; Barth H.-D. ; Brutschy B. A new way to detect noncovalently bonded complexes of biomolecules from liquid micro-droplets by laser mass spectrometry. *Aust. J.* Chem. **2006,** *59*, 109-114.

(46) Kohno J.; Toyama N.; Kondow T. Ion formation to the gas phase by laser ablation on a droplet beam. *Chem. Phys. Lett.* **2006**, 420, 146-150.

(47) Woods E.; Smith G.D.; Dessiaterik Y.; Baer T.; Miller R.E. Quantitative detection of aromatic compounds in single aerosol particle mass spectrometry. *Anal. Chem.* **2001**, 73, 2317-2322.

(48) Lawson S.J.; Murray K.K. Continuous flow infrared matrix-assisted laser desorption/ionization with a solvent matrix. *Rapid Commun. Mass Spectrom.* **2000**, 14, 129-134.

(49) Iguchi Y.; Hazama H.; Awazu K. Continuous flow reduced-pressure infrared laser desorption/ionization mass spectrometry. *Rapid. Commun. Mass Spectrom.* **2017**, 31, 1845-1850.

(50) Laiko V.V.; Taranenko N.I.; Berkout V.D.; Yakshin M.A.; Prasad C.R.; Sang Lee H.; Doroshenko V.M. Desorption/ionization of biomolecules from aqueous solutions at atmospheric pressure using an infrared laser at 3 μm. *J. Am. Soc. Mass Spectrom.* **2002**, 13, 354-361.

(51) Daniel J.M.; Laiko V.V.; Doroshenko V.M.; Zenobi R. Interfacing liquid chromatography with atmospheric pressure MALDI-MS. *Anal. Bioanal. Chem.* **2005**, 383, 895-902.

(52) Rapp E.; Charvat A.; Beinsen A.; Plessmann U.; Reichl U.; Seidel-Morgenstern A.; Urlaub H.; Abel B. Atmospheric pressure free liquid infrared MALDI mass spectrometry : toward a combined ESI/MALDI-Liquid Chromatography interface. *Anal. Chem.* **2009**, 81, 443-452.

(53) Morgner N. ; Kleinschroth T. ; Barth H.-D. ; Ludwig B. ; Brutschy B. A novel approach to analyse membrane proteins by laser mass spectrometry : from protein subunits to the integral complex. *J. Am. Soc. Mass Spectrom.* **2007,** 18, 1429-1438.

(54) Vonck J. ; Pisa K. Y. ; Morgner N. ; Brutschy B. ; Müller V. Three-dimensional structure of $A1A_0$ ATP synthase from the hyperthermophilic archaeon *Pyrococcus furiosus* by electron microscopy. *J. Biol. Chem.* **2009**, *284*, 10110-10119.

(55) Hoffmann J.; Aslimovska L.; Bamann C.; Glaubitz C.; Bamberg E.; Brutschy B. Studying the stoichiometries of membrane proteins by mass spectrometry : microbial rhodopsins and a potassium ion channel. *Phys. Chem. Chem. Phys.* **2010**, 12, 3480-3485.

(56) Hoffmann J. ; Sokolova L. ; Preiss L. ; Hicks D. B. ; Krulwich T. A. ; Morgner N. ; Wittig I. ; Schägger H. ; Meier T. ; Brutschy B. ATP synthases : cellular nanomotors characterized by LILBID mass spectrometry. *Phys. Chem. Chem. Phys.* **2010**, *12 (41)*, 13345-13852.

(57) Morgner N.; Barth H.-D.; Brutschy B.; Scheffer U.; Breitung S.; Göbel M. Binding sites of the viral RNA element TAR and of TAR mutants for various peptide ligands, probed with LILBID : a new laser mass spectrometry. *J. Am. Soc. Mass Spectrom.* **2008**, 19, 11, 1600-1611.

(58) Hoffmann J.; Thorsten L.; Schmidt T.L.; Heckel A.; Brutschy B. Probing the limits of liquid droplets laser desorption mass spectrometry in the analysis of oligonucleotides and nucleic acids. *Rapid Commun. Mass Spectrom.* **2009**, 23, 2176-2180.

(59) Henrich E.; Peetz O.; Hein C.; Laguerre A.; Hoffmann B.; Hoffmann J.; Dötsch V.; Bernhard F.; Morgner N. Analysing native membrane protein assembly in nanodiscs by combined noncovalent mass spectrometry and synthetic biology. *Elife* **2017**, 6 (6), e20954. eLife 2017;6:e20954

(60) Peetz O.; Henrich E.; Laguerre A.; Löhr F.; Hein C.; Dötsch V.; Bernhard F.; Morgner N. Insights into cotranslational membrane protein insertion by combined LILBID-Mass spectrometry and NMR spectroscopy. *Anal. Chem.* **2017**, 89, 22, 12314-12318.

(61) Van Dyck J.F.; Konijnenberg A.; Sobott F. Native mass spectrometry for the characterization of structure and interactions of membrane proteins. *Membrane Protein Structure and Function characterization : Methods and Protocols. Methods Mol. Biol.* **2017**, 1635, 205-232.

(62) Kar U.K.; Simonian M.; Whitelegge J.P. Integral membrane proteins : bottom-up, top-down and structural proteomics. *Expert Rev. Proteome.* **2017**, 14, 715-723.

(63) Schlesinger R. Do it fast : immediate functional testing of membrane pumps expressed into nanodiscs. *Biophys. J.* **2017**, 113, 1177-1178.

(64) Calabrese A.N.; Radford S.E. Mass spectrometry-enabled structural biology of membrane proteins. *Methods* **2018**, 147, 187-205.

(65) Peetz O.; Hellwig N.; Henrich E.; Mezhyrova J.; Dötsch V.; Bernhard F.; Morgner N. LILBID and nESI : Different native mass spectrometry techniques as tools in structural biology. *J. Am. Soc. Mass Spectrom.* **2019**, 30, 1, 181-191.

(66) Stasicki B.; Charvat A.; Faubel M.; Abel B. Visualization of laser-induced liquid micro-jet disintegration by means of high-speed video stroboscopy. *Proceedings of the SPIE 26th International Congress High Speed Photography and Photonics*. **2004**, 5580, 335-346.

(67) Charvat A.; Bögehold A.; Abel B. Time-resolved micro liquid desorption mass spectrometry : mechanism, features, and kinetic applications. *Aust. J. Chem.* **2006**, 59, 81-103.

(68) Terasaki A. Dynamics of clusters initiated by photon and surface impact. *J. Phys. Chem. A* **2007**, 111, 7671-7689.

(69) Terasaki A.; Kondow T. Dynamics of an argon cluster following impulsive excitation studied by molecular-dynamics simulation. *Chem. Phys. Lett.* **2009**, 474, 57-61.

(70) Kohno J.-Y.; Mafuné F.; Kondow T. Ejection of a large neutral cluster from a liquid beam surface following IR laser irradiation. *J. Phys. Chem. A* **2004**, 108, 971-977.

(71) Komatsu K.; Nirasawa T.; Hoshino-Nagasaka M.; Kohno J. Mechanism of protein molecule isolation by IR laser ablation of droplet beam. *J. Phys. Chem. A* **2016**, 120, 1495-1500.

(72) Kohno J.; Kondow T.Trap of biomolecular ions in the gas phase producted by IR-laser ablation of droplet beam. *Chem. Lett.* **2010**, 39, 1220-1221.

(73) Wiley W.C.; McLaren H. Time-of-Flight mass spectrometer with improved resolution. *Rev. Sci. Instr.* **1955**, 26, 1150-1157.

(74) Colby S.M.; King T.B.; Reilly J.P. Improving the resolution of matrix-assisted laser desorption/ionization time-of-flight mass spectrometry by exploiting the correlation between ion position and velocity. *Rapid Commun. Mass Spectrom.* **1994**, 8, 865-868.

(75) Brown R.S.; Lennon J.J. Mass resolution improvement by incorporation of pulsed ion extraction in a matrix-assisted laser desorption/ionization linear time-of-flight mass spectrometer. *Anal. Chem.* **1995**, 67, 1998-2003.

(76) Jensen 0.; Podtelejnikov A.; Mann M. Delayed extraction improves specificity in database searches by Matrix-Assisted Laser Desorption/Ionization peptide maps. *Rapid Commun. Mass Spectrom.* **1996**, 10, 1371-1378.

(77) Rosenfeld D.; Woodley W.L. Deep convective clouds with sustained supercooled liquid water down to -37,5 °C. *Nature* **2000**, 405, 440-442.

(78) Wood S.E.; Baker M.B.; Swanson B.D. Instrument for studies of homogeneous and heterogeneous ice nucleation in free-falling supercooled water droplets. *Rev. Sci. Instr.* **2002**, 73,

(79) Stöckel P.; Weidingers I.M.; Baumgärtel H. Leisner T. Rates of homogeneous ice nucleation in levitated H_2O and D_20 droplets. *J. Phys. Chem. A* **2005**, 109, 2540-2546.

(80) Zilch L. Maze J.T.; Smith JW.; Jarrold M.F. Freezing, fragmentation, and charge separation in sonic sprayed water droplets. *Int. J. Mass Spectrom.* **2009**, 283, 191-199.

(81) Sellberg J.A.; Huang C.; McQuenn T.A.; Loh N.D.; Laksmono H.; Schlesinger D.; Sierrra R.G.; Nordlund D.; Hampton C.Y.; Starodub D.; DePonte D.P.; Beye M.; Chen C.; Martin A.V.; Barty A.; Wikfeldt K.T.; Weiss T.M.; Caronna C.; Feldkamp J.; Skinner L.B.; Seibert M.M.; Messerschmidt M.; Williams G.; Boutet S.; Pettersson L.G.M.; Bogan M.J.; Nilsson A. Ultrafast X-ray probing of water structure below the homogeneous ice nucleation temperature. *Nature*, **2014**, 510, 381-384.

(82) Ando K.; Arakawa M.; Terasaki A. Evaporation of a liquid droplet of ethylene glycol in a vacuum. *Chem. Lett.* **2016**, 45, 961-963.

(83) Goy C.; Potenza M.A.C.; Dedera S.; Tomut M.; Guillerm E.; Kalinin A.; Voss K.-O.; Schottelius A.; Pertridis N.; Prosvetov A.; Tejada G.; Fernández J.M.; Trautmann C.; Caupin F.; Glasmacher U.; Grisenti R.E. Shrinking of rapidly evaporating water microdroplets reveals their extreme supercooling. *Phys. Rev. Lett.* **2018**, 120, 015501

(84) Ando K.; Arakawa M.; Terasaki A. Freezing of micrometer-sized liquid droplets of pure water evaporatively cooled in a vacuum. *Phys. Chem. Chem. Phys.* **2018**, 20, 28435-28444.

(85) Brodeur A.; Chin S.L. Ultrafast white-light continuum generation and self-focusing in transparent condensed media. *J. Opt. Soc. Am. B* **1999**, 16, 637-650.

(86) Favre C.; Boutou V.; Hill S.C.; Zimmer W.; Krenz M.; Lambrecht H.; Yu J.; Chang R.K.; Woeste L.; Wolf J.-P.White-light nanosource with directional emission. *Phys. Rev. Lett.* **2002**, 89, 035002.

(87) Shin D.N. ; Wijnen J.W. ; Engberts J. ; Wakisaka A. On the origin of microheterogeneity : a mass spectrometric study of dimethyl sulfoxide-water binary mixture. *J. Phys. Chem. B* **2001**, 105, 6759-6762.

(88) Dessiaterik Y.; Nguyen T.; Baer T.; Miller R. IR vaporization mass spectrometry of aerosol particles with ionic solutions : the problem of ion-ion recombination. *J. Phys. Chem. A* **2003**, 107, 11245-11252.

(89) Cochran A.G.; Skelton N.J.; Starovasnik M.A. Tryptophan zippers : stable, monomeric beta-hairpins. *Proc. Natl. Acad. Sci. U.S.A.* **2001**, 98, 5578-5583.

(90) Jørgensen T.J.D; Hvelplund P.; Andersen J.U.; Roepstorff P. Tandem mass spectrometry of specific vs. nonspecific noncovalent complexes of vancomycin antibiotics and peptide ligands. *Int. J. Mass. Spectrom.* **2002**, 219, 659-670.

(91) Diana J.; Visky D.; Hoogmartens J.; Van Schepdael A.; Adams E. Investigation of vancomycin and related substances by liquid chromatography/ion trap mass spectrometry. *Rapid Commun. Mass Spectrom.* **2006**, 20, 685-693.

(92) Perkins H.R. Specificity of combination between mucopeptide precursors and vancomycin or ristocetin. *Biochem. J.* **1969**, 111, 195-205.

(93) Liu J.; VolkK.J.; Lee M.S.; Pucci M.; Handwerger S. Binding studies of vancomycin to the cytoplasmic peptidoglycan precursors by affinity capilliary electrophoresis. *Anal. Chem.* **1994**, 66, 2412-2416.

(94) Poully J.C.; Lecomte F.; Nieuwjaer N.; Manil B.; Svhermann J.P.; Desfrançois C.; Calvo F.; Grégoire G. Probing the specific interactions and structures of gas-phase vancomycin antibiotics with cell-wall precursor through IRMPD spectroscopy. *Phys. Chem. Chem. Phys.* **2010**, 12, 3606-3615.

(95) Poully J.C.; Lecomte F.; Nieuwjaer N.; Manil B.; Schermann J.P.; Desfrançois C.; Grégoire G.; Ballivian R.; Chirot F.; Lemoine J.; Calvo F.; Antoine R.; Dugourd P. Combining ion mobility mass spectrometry and infrared

multiphoton dissociation spectroscopy to probe the structure of gas-phase vancomycin-$Ac_2{}^LK^DA^DA$ non-covalent complex. *Int. J. Mass Spectrom.* **2010**, 297, 28-35.

(96) Dahl D.A. SIMION for the personal computer in reflection. *Int. J. Mass Spectrom.* **2000**, 200, 3-25.

(97) Sugiyama A.; Nakajima A. Dual IR shattering of a water microdroplet. *Appl. Phys. A* **2012**, 109, 31-37.

(98) Schneider B.B. ; Douglas D.J. ; Chen D.D.Y. Collision-induced dissociation of bradykinin ions in the interface region of an ESI-MS. *J. Am. Soc. Mass Spectrom.* **2001**, 12, 772-779.